Critical Contact Residues That Mediate Polymerization of Nematode Major Sperm Protein

Antonio del Castillo-Olivares and Harold E. Smith*

Center for Advanced Research in Biotechnology, University of Maryland Biotechnology Institute, Rockville, Maryland 20850

Abstract   The polymerization of protein filaments provides the motive force in a variety of cellular processes involving cell motility and intracellular transport. Regulated assembly and disassembly of the major sperm protein (MSP) underlies amoeboid movement in nematode sperm, and offers an attractive model system for characterizing the biomechanical properties of filament formation and force generation. To that end, structure-function studies of MSP from the nematode *Caenorhabditis elegans* have been performed. Recombinant MSP was purified from *Escherichia coli* using a novel affinity chromatography technique, and filament assembly was assessed by in vitro polymerization in the presence of polyethylene glycol. Prior molecular studies and structure from X-ray crystallography have implicated specific residues in protein–protein interactions necessary for filament assembly. Purified MSP containing substitutions in these residues fails to form filaments in vitro. Short peptides based on predicted sites of interaction also effectively disrupt MSP polymerization. These results confirm the structural determination of intermolecular contacts and demonstrate the importance of these residues in MSP assembly. J. Cell. Biochem. 104: 477–487, 2008.   © 2007 Wiley-Liss, Inc.

Key words: filament polymerization; cytoskeleton; nematode sperm; cell motility; peptide inhibitor

Dynamic modulation of protein polymerization is a recurring motif in the mechanisms mediating motility on the cellular and intracellular level. In many instances, the directed assembly of protein filaments is thought to provide the motive force. Intracellular pathogens such as Listeria and Shigella possess cell surface proteins that polymerize actin within the host to propel themselves through the cytosol [Stevens et al., 2005; Carlsson and Brown, 2006]. Assembly of actin filaments also drives diverse cellular processes like neuronal growth cone migration, phagocytosis, and motility in crawling cells [Pollard and Borisy, 2003; Disanza et al., 2005]. The dynamics of filament assembly play a critical role even in those functions (e.g., chromosome segregation) that are mediated primarily by motor proteins. Therefore, analysis of the biomechanical properties of filament polymerization provides insights into force generation at the molecular level.

The crawling movement of nematode sperm is an appealing model for the study of cell motility based on filament assembly. Sperm motility does not depend upon the typical components actin or tubulin (which are essentially absent from the mature spermatozoa), but instead employs the novel major sperm protein (MSP) [Nelson et al., 1982; Roberts et al., 1989]. MSP, a basic protein of ~14 kDa, is highly conserved among nematodes and typically encoded by a multigene family [Burke and Ward, 1983; Scott et al., 1989]. Treadmilling of the sperm pseudopod occurs by regulated polymerization of MSP at its leading edge and disassembly at its base [Roberts and Ward, 1982; Sepsenwol et al., 1989]. Although MSP acts as an extracellular signaling molecule to stimulate oocyte maturation and egg-laying rate [Miller et al., 2001], its only known role within the sperm is pseudopod movement. Therefore, MSP-based motility can be studied in isolation from other cellular processes, whereas the myriad functions of actin and tubulin greatly complicate the analysis of these components.

MSP polymers assume different architectures within the cell during the course of sperm development. Detailed cytological studies of nematode sperm have been reported for the soil-dwelling *Caenorhabditis elegans* as well as the intestinal parasite *Ascaris suum* [Ward et al., 1981; Ward and Klass, 1982; Roberts et al., 1986]. Differentiation of germ line stem cells gives rise to primary spermatocytes that separate from the syncytial cytoplasmic core. As the primary spermatocyte initates meiosis, MSP begins to assemble into paracrystalline arrays called fibrous bodies. These structures grow in size until the second meiotic division is complete. The fibrous bodies then segregate into the four haploid spermatids as they separate from the residual body; at that point, MSP depolymerizes and becomes distributed throughout the cytosol. Spermatids remain as spherical, immotile cells until an extracellular signal induces spermiogenesis, or sperm activation. Activation promotes the reinitiation of MSP polymerization, which drives the dynamic formation of thin cell-surface projections called spikes or filopodia [Shakes and Ward, 1989; Rodriguez et al., 2005]. These structures lengthen and retract rapidly, then are replaced by a complex cytoskeletal assembly of MSP within the pseudopod of the crawling spermatozoon.

Polymerization is an intrinsic property of MSP, as the addition of polyethylene glycol (PEG) or water-miscible alcohol to purified protein is sufficient to drive assembly [King et al., 1992]. Polymerization in the presence of PEG results in the formation of tiny, needle-like crystals visible by light microscopy. Negatively stained EM images of transverse sections reveal sinusoidal striations with an axial repeat of 9 nm. This pattern is the product of parallel arrays of helical polymers termed subfilaments. Treatment with alcohol also generates helical MSP subfilaments, which are further assembled into a variety of higher order structures [King et al., 1994; Stewart et al., 1994]. Pairs of subfilaments are entwined to form helical filaments, multiple filaments (usually two or three) are bundled to produce helical macrofibers, and fiber rafts or meshlike mats are built from filaments and/or macrofibers. In vivo polymerization of MSP in the pseudopod exhibits a similar hierarchy of helical assemblies. MSP polymers within intact spermatozoa are stabilized by PEG treatment, and negative staining reveals the presence of subfilaments, filaments, and fibers [King et al., 1992]. Although the fibers appear to differ in some aspects, subfilaments and filaments produced either in vivo or in vitro are indistinguishable from each other.

The structure of MSP has been determined at atomic-level resolution. X-ray crystallographic analyses of MSP from both *A. suum* [Bullock et al., 1996] and *C. elegans* [Baker et al., 2002] yield nearly identical structures, with the monomer consisting of seven beta strands in an immunoglobulin-type fold. These structures also provide details of intermolecular contacts thought to underlie polymerization. MSP within the crystals formed symmetrical dimers, consistent with earlier solution studies [Haaf et al., 1996], and the dimers were assembled into parallel arrays of helical subfilaments. From these data, critical residues were identified at both the dimerization interface and the subfilament assembly interface. Interhelical contact residues were proposed as putative sites of filament and/or fiber assembly.

Functional roles for the proposed dimer and subfilament assembly interfaces are independently supported by mutational analyses. The yeast two-hybrid system was employed to identify random missense mutations that disrupt MSP–MSP interaction [Smith and Ward, 1998]. These mutations were further characterized biochemically for defects in dimer formation. Size exclusion chromatography of bacterially expressed protein revealed two classes of mutations: those that abrogated dimerization and those that, like wild type MSP, formed stable dimers. The differences in dimerization were readily interpretible in light of the crystal structure. Dimer-defective mutations all mapped to contact residues between MSP monomers. The mutations that had no effect on dimerization fell outside of that interface, but were located near the site of subfilament assembly. The side chains of those residues were mostly oriented toward the interior of the protein, so the proposed mechanism for the interaction defect was through localized distortion of the subfilament assembly interface.

An understanding of the interactions involved in MSP polymerization is a critical step in determining the mechanics of force generation. We have used in vitro polymerization of purified protein in the presence of PEG to characterize MSP assembly. Functional

sites were identified by specific missense mutations that disrupt assembly or by peptides that competitively inhibit polymerization. These data confirm the predictions of earlier structural studies, and the reagents generated in this work will prove useful in dissecting the mechanics of filament assembly that underlie force generation in this model system.

RESULTS

Affinity Chromatography Purification of MSP

Prior studies [Smith and Ward, 1998] utilized ion exchange chromatography to purify wild type MSP expressed in *Escherichia coli*, but protein from MSP genes containing missense mutations exhibited different binding and elution characteristics during preliminary attempts at purification. Therefore, a novel one-step affinity chromatography system [Ruan et al., 2004] was employed to eliminate the need to optimize purification parameters for the mutant MSPs. The technology consists of an engineered variant of the protease subtilisin that exhibits selective substrate specificity plus regulated catalytic activity. DNA encoding the prodomain of subtilisin is fused to the gene for the protein of interest, and the fusion protein is expressed in bacteria. Clarified cell lysate is applied to the column-immobilized subtilisin, which binds specifically and with high affinity to the prodomain. The prodomain contains the cleavage recognition site for subtilisin, and proteolysis is activated by the addition of fluoride ions to release the target protein. The prodomain is retained on the column, so the eluate contains only the purified protein of interest.

The subtilisin prodomain proR8FKAM was amplified from donor plasmid pG58 [Ruan et al., 2004] and inserted into bacterial expression vectors containing the gene encoding wild type or missense mutations of MSP (pET-MSP or pET-MSP*) [Smith and Ward, 1998]. The resulting pET-PRO-MSP expression plasmids were designed so that cleavage of the prodomain would produce native MSP with no additional residues. Prior work had identified optimal growth conditions for expression of soluble MSP; the same conditions were used for the production of PRO-MSP fusion proteins. Soluble cell lysates were examined by SDS/PAGE and Coomassie blue staining and, after induc-

tion, contained a predominant band of the expected molecular weight (see Fig. 1, lane 1). Those lysates were fractionated by subtilisin chromatography.

Figure 1 shows a typical purification profile and SDS/PAGE/Coomassie staining of selected fractions for wild type MSP. The elution fractions (lanes 4–6) clearly indicate a single protein of the correct molecular weight with little contaminating material present. Western blotting with monoclonal antibodies specific for MSP confirmed the identity of the purified protein (data not shown). Similar results were obtained with MSPs containing the single amino acid substitutions used in this study. The purified proteins were characterized by in vitro polymerization assays.

Assembly of MSP Subfilaments In Vitro

MSP assembly is not associated with conformational changes in either the monomer or dimer structure [Bullock et al., 1996; Haaf et al., 1996, 1998], so polymerization is thought to be regulated at the level of subfilament formation. Since MSP subfilaments have the same structure whether produced in vivo or in vitro, we chose the latter method to investigate this critical step in polymerization. Prior work with
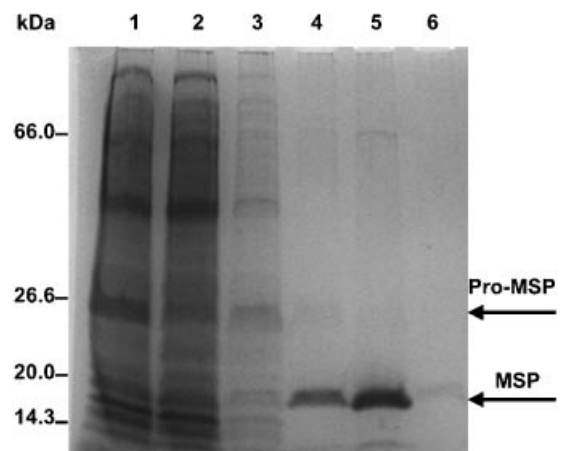
Fig. 1. MSP purification by subtilisin affinity chromatography. Soluble protein extract from *Escherichia coli* expressing the PRO-MSP fusion gene was fractionated as described in Materials and Methods Section. Shown are various fractions separated by SDS/PAGE and stained with Coomassie blue to visualize proteins. **Lane 1**, total soluble extract; **lane 2**, column flowthrough; **lane 3**, column wash; **lanes 4–6**, column elution fractions. Molecular weights of protein standards are indicated on the left. Positions of the PRO-MSP and cleaved MSP proteins are indicated on the right.

MSP from *A. suum* demonstrated that treatment with PEG is sufficient to promote assembly into needle-like crystals composed of parallel arrays of subfilaments. These crystalline needles are readily visible by light microscopy, so polymerization of wild type MSP from *C. elegans* was characterized using this simple and rapid technique.

Our initial filament assembly assay replicated the same conditions reported for MSP from *A. suum* (3 mg/ml protein, 15% PEG, average MW 18,500) [King et al., 1992]. Figure 2A is a DIC Nomarski image of the crystalline needles of MSP produced by PEG treatment. Controls with BSA in lieu of MSP (Fig. 2B) or with PEG alone (Fig. 2C) failed to generate crystals. Polymerization of MSP is nearly instantaneous upon addition of PEG, as indicated by conversion of the clear protein solution to an opaque suspension of crystals. Attempts to observe the polymerization process by mixing the MSP and PEG on the microscope slide were unsuccessful because crystal formation was complete within the few seconds it took to adjust the focal plane. MSP polymerization is also rapidly reversible; when crystalline MSP was resuspended in buffer lacking PEG, needles
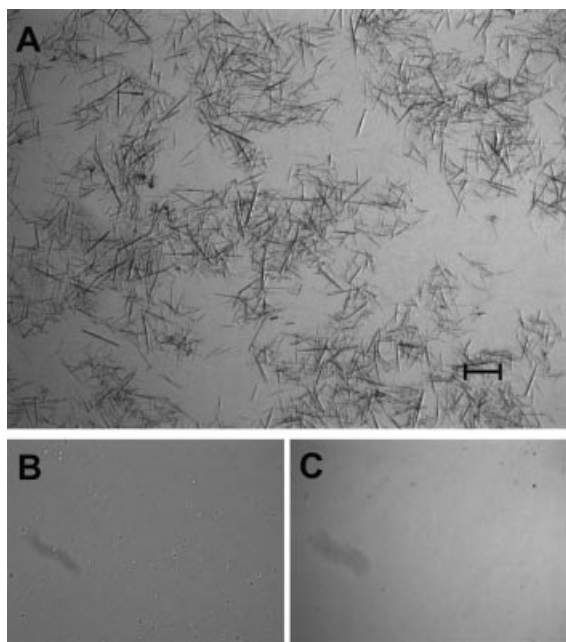
Fig. 2. In vitro polymerization of MSP. Shown are Nomarski differential interference contrast photomicrographs of filament assembly assays in the presence of PEG. **A**: Experimental sample with MSP. Note the large number of crystalline needles, indicative of assembly. **B**: Control sample with bovine serum albumin. **C**: Control with no protein. Scale bar, 10 µm.

were no longer visible by microscopy. Likewise, in vitro assembly of *A. suum* MSP is both rapid and reversible [King et al., 1992]. Thus, the ability to polymerize is an intrinsic property of *C. elegans* MSP and shares many similarities with that of *A. suum*.

Wild type MSP was tested for crystal formation under various combinations of protein concentration, PEG concentration, and PEG molecular weight. The concentrations of both PEG and MSP were the most critical variables in promoting polymerization. For MSP at 5 mg/ml, no crystals were observed at the lowest PEG concentration of 5% (data not shown), while crystals were obtained in 15% PEG and 10% PEG at all molecular weights (Fig. 3, rows 1 and 2). When the MSP concentration was reduced to 1 mg/ml, a minimum of 15% PEG was required for crystal formation (Fig. 3, row 3). MSP polymerization was least affected by the molecular weight of PEG; only the lowest weight tested (MW 3,500) failed to produce crystals under conditions (15% PEG and 1 mg/ml MSP) where those with higher molecular weights succeeded. However, PEG molecular weight had a more qualitative effect on MSP assembly. In general, the lower MW species produced fewer but larger (both longer and wider) crystalline needles than PEGs of higher MW (particularly evident in Fig. 3, second row). Protein concentration also affected crystal formation, with fewer but larger crystals obtained at the lower protein concentration (compare rows one and three in Fig. 3). Taken together, the data indicate that polymerization of MSP in the presence of PEG is robust across a range of conditions.

Assembly Defects of MSP Mutations

The crystal structure of *C. elegans* MSP has been determined at high resolution and reveals multiple sites of interaction [Baker et al., 2002]. The protein exhibits an immunoglobulin-like fold comprised of seven beta strands. The dimerization interface (by published nomenclature, D1) is symmetrical and consists of strands a_2 (residues 14–23; all positions in this study are +1 to those used to describe the crystal structure) and b (residues 25–33) and the penultimate asparagine at position 126. The assembly interface for the helical subfilament (D2) is between extended g strands (residues 111–120) in antiparallel orientation. The protein crystallized as parallel but individual
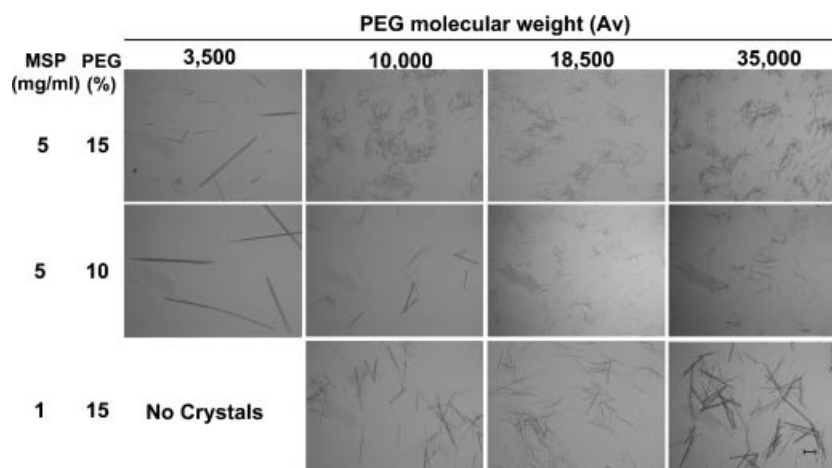
Fig. 3. In vitro polymerization of MSP under various conditions. Shown are Nomarski differential interference contrast photomicrographs of filament assembly assays. Changes in MSP protein concentration, percentage of PEG, and average molecular weight of PEG are indicated for each panel. Scale bar, 10 μm.

subfilaments rather the entwined pairs of subfilaments thought to comprise filaments. However, crystal contacts between the subfilaments were interpreted as likely interaction sites for bona fide filaments. Those five sites of contacts contained multiple residues distributed throughout the peptide chain and were labeled H1 through H5.

Missense mutations that disrupt MSP–MSP interaction were identified previously in a yeast two-hybrid screen, and a subset were assayed for MSP dimerization in solution by size exclusion chromatography [Smith and Ward, 1998]. Four alleles from that screen were selected for further characterization on the basis of that work as well as the crystal structure of *C. elegans* MSP. The positions of those amino acid substitutions in the context of two MSP dimers are diagramed in Figure 4. The asparagine residue at position 126 (shown in red) maps to the dimerization interface D1 (green) and forms a hydrogen bond with lysine at residue 17. Mutation of this residue to lysine (abbreviated N126K) was shown to disrupt dimer formation of bacterially expressed MSP. Mutations K119E, I123N, and Y125H (indicated in blue) fall within or adjacent to subfilament assembly interface D2 (cyan). Those mutations had no effect on dimerization when assessed by size exclusion chromatography. Those residues do not make intermolecular contacts in the MSP crystal, and so were interpreted to disrupt interaction through D2 by distortion of the *g* strand.

For each of the four mutations, purified MSP containing a single amino acid substitution was assayed for PEG-promoted polymerization. The assembly assay was first validated with the dimerization-defective mutation N126K. Subfilaments are assembled from MSP dimers, so disruption of dimerization is strongly predicted to block polymerization. Initial trials consisted of 5 mg/ml protein and 15% PEG 18,500, conditions that produce abundant crystalline needles for wild type MSP from *A. suum* and *C. elegans*. As expected, the N126K mutation produced no crystals; only disordered protein
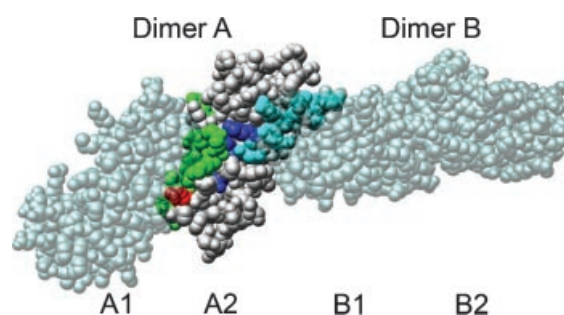
Fig. 4. Structure of MSP assembly interfaces and amino acid substitutions. Four monomers of MSP (A1, A2, B1, and B2) are illustrated. Relevant intermolecular contacts are highlighted only in subunit A2 for the sake of clarity. The dimerization interface between A1 and A2 is shown in green. The subfilament assembly interface between A2 and B1 is shown in cyan. The amino acid substitution N126K is shown in red; amino acid substitutions K119E, I123N, and Y125H are shown in blue. The figure was generated from coordinates *1GRW* deposited at the RCSB Protein Data Bank [Berman et al., 2000] using the UCSF Chimera package [Pettersen et al., 2004].

TABLE I. Amino Acid Substitions That Disrupt MSP Assembly

Amino acid change[a]	Defective interaction[b]	Polymerization?[c]
N126K	Dimerization	No (aggregates)
K119E	Subfilament assembly	No
I123N	Subfilament assembly	No
Y125H	Subfilament assembly	No

Summary of the single amino acid substitutions tested for their effect on MSP polymerization. Mutations encoding these substitutions were isolated in a previous screen for interaction-defective MSPs [Smith and Ward, 1998].
[a]Amino acids are denoted by conventional one-letter nomenclature. Substitutions are indicated by the wild type residue, position within MSP, and substituted residue.
[b]Assignment of interaction interface is predicted from the crystal structure of *Caenorhabditis elegans* MSP [Baker et al., 2002].
[c]MSP polymerization was assessed by the appearance of crystalline needles in 15% PEG (MW$_{avg}$ 18,500) at 5 mg/ml protein concentration.

aggregates were observed. The assay was then repeated for the three mutations in the putative subfilament assembly interface; the results were indistinguishable from controls that lacked MSP (summarized in Table I). Different protein concentrations (1 and 5 mg/ml), PEG concentrations (5%, 10%, and 15%), and PEG molecular weights (3,500, 10,000, 18,500, and 35,000) were tested in all possible combinations in an effort to facilitate MSP assembly (data not shown). No conditions were identified that promoted needle formation for any of the four mutant MSPs examined. Therefore, mutations that disrupted MSP–MSP interaction in the two-hybrid screen also block in vitro assembly of the protein. Furthermore, the results indicate that both the D1 and D2 sites of interaction are necessary for MSP polymerization in this assay.

Peptide Inhibitors of MSP Assembly

Molecules that bind to sites of MSP interaction are predicted to interfere with in vitro polymerization and inhibit the formation of needles in the presence of PEG. Small molecule inhibitors of MSP assembly have yet to be identified, but a fragment of MSP containing an interaction domain might function in the same manner. This same strategy was employed successfully to identify a 10 residue peptide from HIV reverse transcriptase that blocks enzyme dimerization in vitro and viral replication in infected cell culture [Morris et al., 1999]. Therefore, peptides based on the various sites of MSP–MSP interaction (described in Table II and Fig. 5) were screened for the ability to block in vitro polymerization of wild type protein.

The analysis of mutant MSPs described above demonstrates that defects in either dimer formation or subfilament assembly are sufficient to disrupt in vitro polymerization. Therefore, peptides were designed that contain much of the dimerization interface D1 between MSP monomers (peptide PI-1; green in Fig. 5) or that span the entire subfilament assembly site D2 (peptide PI-2; cyan in Fig. 5). HPLC analysis revealed a predominant peak for each peptide tested, and mass spectrometry was consistent with the predicted molecular weight (data not shown). Purified wild type MSP was mixed with

TABLE II. Peptide Inhibition of MSP Polymerization in PEG

Peptide	Target interface[a]	Peptide sequence[b]	Residues[c]	Concentration[d] (mM)
PI-1	D1	QTQPGTKIVFNAPYDD	11–26	6.6
PI-2	D2	QGDGMVRRKNLPIEYN	111–126	1.25
PI-3	H1, H2, H5	NTPDGAAKQFRREWF	96–110	3.3
PI-4	H2, H3, H4	DAFAFGQEDTNNDRI	76–90	3.3
C1	None	SIPPEVKFNKPFVFLMIEQNTKSPLFMGKVVNPTQK	N/A	N/A

List of peptides tested for inhibition of MSP polymerization in the presence of PEG. The concentration of peptide used in each assay is described in Figure 6.
[a]Target interface employs the nomenclature used to describe sites of interaction in the crystal structure of *C. elegans* MSP [Baker et al., 2002]. D1, dimerization interface; D2, subfilament assembly interface; H1–H5, filament assembly contacts.
[b]Peptide sequence is shown in NH$_2$ to COOH orientation. Control peptide C1 is from human α-1-antitrypsin.
[c]Residue positions of the indicated peptide within MSP; positions are +1 relative to those listed in the crystal structure [Baker et al., 2002]. N/A, not applicable.
[d]Minimum effective concentration at which peptide inhibitor completely eliminates MSP polymerization. N/A, not applicable.
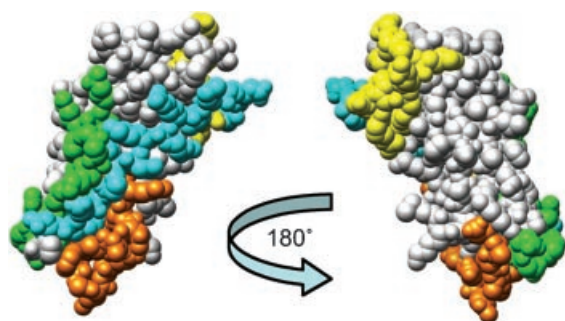
Fig. 5. Structural location of MSP peptide inhibitors. One monomer of MSP is illustrated. The diagram on the left is in the same orientation as subunit A2 in Figure 4. The diagram to the right is rotated 180° about the *Y*-axis. Peptide PI-1 is shown in green, peptide PI-2 in cyan, peptide PI-3 in yellow, and peptide PI-4 in orange. Amino acid sequences of the peptides, and their residue positions in MSP, are listed in Table II.

peptide at different concentrations and tested to identify the minimum concentration necessary to abolish filament formation in PEG (Fig. 6). Both peptides PI-1 and PI-2 interfered with MSP needle assembly, though to varying degrees. The effective concentration of peptide inhibitor PI-1 was fivefold greater than that of PI-2 (6.6 mM vs. 1.25 mM) and the assay still contained a small number of tiny crystals. In contrast, peptide PI-2 completely abolished needle formation at the lower concentration. Reducing the concentration of peptide inhibitor by 50% had the same qualitative effect as reducing the concentration of MSP, producing fewer but larger crystals (data not shown). A control peptide unrelated to MSP (C-1) failed to
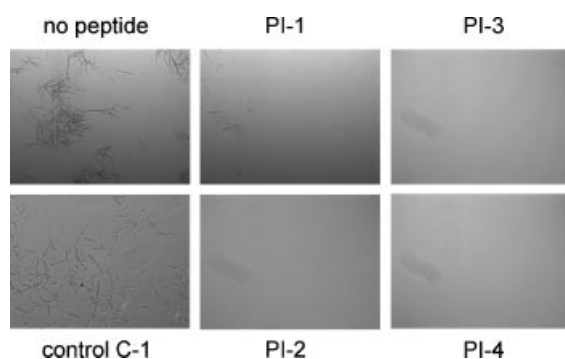
Fig. 6. Peptide inhibition of in vitro polymerization of MSP. Shown are Nomarski differential interference contrast photomicrographs of filament assembly assays. Peptide inhibitors (described in Table II) were mixed with purified MSP prior to the addition of PEG. The final concentration of peptides PI-1 and control C-1 is 6.6 mM; peptides PI-3 and PI-4, 3.3 mM; and peptide PI-2, 1.25 mM.

block crystal formation, demonstrating that the inhibition of polymerization by PI-1 and PI-2 is specific to the peptide sequence.

Peptides derived from higher-order sites of MSP assembly might also suffice to inhibit in vitro polymerization, so two additional peptides were designed based on the predicted sites of interaction between subfilaments to form filaments and/or fibers [Baker et al., 2002]. Peptide PI-3 (Fig. 5, shown in yellow) overlaps residues in the filament assembly sites H1, H2, and H5, and peptide PI-4 (Fig. 5, in orange) contains residues from filament assembly sites H2, H3, and H4. Each of these peptides was able to disrupt the formation of crystalline needles at a concentration intermediate between those of PI-1 and PI-2 (Fig. 6). The residues of MSP contained in PI-3 and PI-4 are not implicated in either dimerization or subfilament assembly, which suggests that the contacts required for assembly in this assay are the same as those utilized for filament and/or fiber formation.

DISCUSSION

The present work utilizes in vitro polymerization of MSP to demonstrate the functional significance of residues of the protein needed for assembly. A novel affinity purification system allowed one-step isolation of recombinant proteins for polymerization assays. Addition of PEG promoted assembly of wild type MSP into needle-like crystals, and assembly was robust across a variety of conditions. Missense mutations known to disrupt MSP–MSP interaction also abrogated in vitro polymerization, and peptides derived from small segments of MSP likewise blocked assembly. These results identify residues that serve as sites of interaction critical for the polymerization of MSP, information that is a necessary prerequisite for understanding the properties of force generation that drive motility in this system.

PEG treatment provides a simple and rapid technique for qualitative assessment of MSP polymerization, and the results obtained in these experiments are consistent with independent methods used to identify the sites of interaction. The evidence for the D1 dimerization and D2 subfilament assembly interfaces is particularly compelling. The missense alleles used in this study were originally isolated by random mutagenesis in a functional screen for interaction-defective MSPs in a yeast two-hybrid

screen, and the majority of mutations recovered in that screen mapped to the dimerization or subfilament assembly regions. The same mutations disrupted needle formation by PEG addition, which indicates the functional importance of those residues for MSP polymerization. Therefore, PEG-promoted assembly in vitro occurs via those same intermolecular interactions thought to mediate MSP polymerization in vivo.

Inhibition of needle formation by short peptides was used as a second method to define surfaces critical for MSP assembly. Peptides that are conformationally similar to assembly interfaces are predicted to bind to and disrupt sites of protein–protein interaction. Potential peptide inhibitors were based on intermolecular contacts predicted from the X-ray crystal structure of *C. elegans* MSP. These peptides were tested for the ability to block in vitro polymerization of MSP.

Peptides composed of the dimerization or subfilament interfaces (PI-1 and PI-2, respectively) effectively interfered with MSP needle assembly, demonstrating the role of these interfaces in polymerization. Disruption of needle formation was sequence-specific, as an unrelated peptide had no effect. The two peptides differed in their ability to disrupt assembly. The relative inefficiency of inhibition by PI-1 might arise from a difference in the peptide conformation outside the context of MSP, or may reflect the importance of residues that comprise the dimerization interface but are absent in this peptide. Specifically, missense mutations indicate that asparagine 126 is critical for dimer formation, but this residue is not contained in peptide PI-1. Alternatively, the stability ($K_d < 5 \times 10^{-8}$) of MSP–MSP dimers in solution [Haaf et al., 1996] might reduce the accessibility of this interface to peptide PI-1. If so, extended preincubation with the peptide prior to addition of PEG would be predicted to increase assembly inhibition in a time-dependent manner.

Peptide inhibitors based on structural predictions of filament/fiber assembly interfaces (PI-3 and PI-4) also disrupted needle formation. The assignments of these sites are more speculative, as the crystals used for X-ray diffraction assembled as parallel arrays of individual subfilaments rather than the entwined pairs that comprise native filaments. These residues might reflect crystal contacts instead of filament assembly sites, although the authors favored the latter explanation. If MSP polymerization by PEG mimics crystal formation processes, as seems likely, then peptides that block crystal contacts would be expected to disrupt needle assembly. Future studies of bona fide filaments and fibers will be needed to resolve this issue.

PEG-promoted polymerization offers multiple advantages as a simple and qualitative test for MSP assembly. The current study demonstrates its suitability for assessing inhibitors of MSP polymerization, and the assay could be readily adapted for high-throughput screening of molecular compound libraries. Inhibition of crystal formation would be detectable by light spectrometry as a decrease in light scattering, or by light microscopy and automated image analysis of needle formation. Small molecule inhibitors would allow in vivo dissection of MSP assembly and pseudopod dynamics in the crawling sperm. This in vitro assay also provides a means of characterizing missense mutations with defects in MSP assembly. Such mutations cannot be assessed in vivo, because MSP is encoded by a multigene family (in the case of *C. elegans*, a total of 28 nearly identical genes) [Burke and Ward, 1983; Klass et al., 1984; Ward et al., 1988]. The presence of multiple wild type copies precludes the detection of interaction-defective mutations by classical genetic screens.

Although in vitro assembly of MSP is suitable for some applications, it does not reproduce in vivo dynamics or polymer ultrastructure beyond the level of subfilament formation. As is true for actin and other filament proteins, in vivo polymerization of MSP and formation of the resulting cytoskeletal architecture is controlled by additional protein components. A reconstituted cell-free MSP assembly system derived from *A. suum* sperm lysate has been developed that accurately replicates in vivo motility [Italiano et al., 1996]. Critical components (in addition to MSP) include membrane vesicles derived from the leading edge of the pseudopod, a cytosolic fraction, and ATP. Video microscopy indicates that the vesicles nucleate MSP polymerization, producing fibers that propel the vesicles forward at rates approaching those observed for pseudopod movement. More recently, a similar system has been reported that replicates filopodia formation [Miao et al., 2007].

Individual proteins that regulate MSP assembly have been identified in the cell-free system. MPOP, a 48 kDa integral membrane protein, is the only vesicle-derived constituent essential for MSP polymerization, and its activity appears to be regulated by tyrosine phosphorylation [LeClaire et al., 2003]. Two of the cytosolic components are MFP2, a 38 kDa protein that promotes MSP assembly, and MFP1, a complex of three related 15–16 kDa proteins that inhibits MSP polymerization [Buttery et al., 2003]. MFP1 and/or MFP2 cannot replace the cytosolic fraction to reconstitute assembly, so additional factors (e.g., the kinase and phosphatase that regulate MPOP phosphorylation) remain to be identified.

The reconstituted system complements the PEG polymerization assay; although it replicates in vivo motility, it is not suitable for inhibitor or mutational screens. To combine the advantages of the two assays, peptides based on *A. suum* MSP but comprising the identical regions as the current study could be assayed in the reconstituted system for effects on parameters such as assembly rates, vesicle motility, and fiber architecture. Such inhibitory peptides are likely to alter MSP polymerization properties much like effects reported for the MFP1 protein complex [Buttery et al., 2003]. Addition of purified MFP1 to the reconstituted system slowed the rate of fiber growth and also decreased density and diameter of the growing fiber. MFP1 colocalized with MSP fibers, although the site of interaction was not determined. An advantage of inhibitory peptides is that assembly can be modulated at a particular site of interaction without disrupting the other contacts. Such tools might prove useful in determining if specific assembly steps occur sequentially or concurrently, as well as identifying which interaction(s) is rate-limiting for MSP polymerization.

The analysis of interaction-defective mutations necessitated the use of *C. elegans* MSP in the current study, because no such mutants are available for *A. suum*. A reconstituted motility system has not yet been developed for *C. elegans* but, given the high degree of conservation between MSPs from the two species, it might be possible to replace the *A. suum* MSP with that of *C. elegans* and have it function properly. Alternatively, the mutations identified in *C. elegans* MSP could be engineered into the *A. suum* gene, expressed and purified as above,

then tested in the reconstituted system. All of the mutations are predicted to disrupt motility in this assay, but one or more combinations of wild type and mutant MSPs might modulate specific aspects of filament formation. For example, incorporation of MSP defective in subfilament assembly into the growing fiber might function in a manner analogous to capping protein during actin polymerization. Decreasing the mean chain length of the MSP subfilament might alter one or more of the properties, such as fiber density, that contribute to force generation and motility.

MATERIALS AND METHODS

Plasmids

The pET-MSP plasmids for T7-inducible expression of MSP (wild type and mutant) have been described previously [Smith and Ward, 1998]. The subtilisin prodomain variant pro-R8FKAM was amplified by PCR from plasmid pG58 [Ruan et al., 2004] with sequence-specific primers R8-5′ (5′-AAA**CCATGG**GAGGGAAA-TCAAACGG-3′) and R8-3′ (5′-TTT**CCATGG**-CTTTAAATACTTTGTCTTC-3′). Primers were designed to introduce *Nco*I restriction sites (in bold) overlapping either the prodomain start codon (underlined in R8-5′) or the terminal methionine codon (underlined in R8-3′) of the subtilisin cleavage recognition sequence Phe-Lys-Ala-Met. Following amplification, the PCR product was digested with *Nco*I and ligated into the corresponding pET-MSP plasmids digested with *Nco*I to generate wild type or mutant pET-PRO-MSP plasmids. Diagnostic restriction digests followed by automated cycle sequencing were used to confirm the desired constructs.

Bacterial Expression of MSP

Optimal conditions for pET-MSP induction had been determined previously [Smith and Ward, 1998], and the same conditions were employed in this study. Briefly, each pET-PRO-MSP plasmid was transformed into *E. coli* strain BL21(DE3) that also contained plasmid pLysS to minimize background expression [Studier, 1991]. Cultures were grown at 37°C for wild type MSP or 25°C for mutant MSPs in LB medium until $A_{600} = 0.5-0.6$, then protein expression was induced with IPTG at 1 mM final concentration. Cells were harvested 6 h

post-induction by centrifugation, and PRO-MSP accumulation assessed by SDS/PAGE and Coomassie blue staining. Cell pellets were resuspended in 100 mM KPO_4 buffer, pH 7.2/0.1 mM EDTA. Efficient lysis was attained by two freeze-thaw cycles, treatment with lysozyme and DNase I, and sonication. Lysates were clarified by two rounds of centrifugation (15 min at 10,000g, then 1 h at 100,000g).

Protein Purification of MSP

PRO-MSP proteins were fractionated by subtilisin affinity chromatography (affinity column graciously provided by Philip Bryan). Engineered subtilisin variant S189 [Ruan et al., 2004] had been covalently coupled to a 5 ml N-hydroxysuccinimide-Sepharose HiTrap column (Amersham Biosciences). Clarified lysate was loaded onto the affinity column pre-equilibrated in 100 mM KPO_4 buffer, pH 7.2/0.1 mM EDTA (buffer A), then washed with five column volumes of the same buffer, three volumes of 1 M KPO4, pH 7.2, and five volumes buffer A to remove unbound proteins. Subtilisin cleavage of bound PRO-MSP was triggered by one volume of buffer A containing 100 mM KF, which was allowed to remain on the column for 10 min. Purified MSP was eluted with buffer A (collected in three individual column volumes). The column was stripped of bound prodomain with 0.1 N H_3PO_4 and immediately regenerated with buffer A. Elution fractions containing MSP were pooled and dialyzed against buffer A, then concentrated to between 15 and 20 mg/ml via Centricon-10 (Millipore). Some samples were supplemented with Triton X-100 at 0.1% final concentration to minimize aggregation at high concentrations.

In Vitro MSP Assembly

Wild type or mutant MSP was diluted in buffer A so that mixture with PEG would yield 5 or 1 mg/ml protein final concentration. PEG was likewise prepared in buffer A to produce final concentrations of 5%, 10%, or 15% after addition to MSP. Peptides used for inhibition assays (prepared by Bio-Synthesis, Inc., Lewisville, TX) were resuspended in water (control C-1, and inhibitors PI-1, -2, and -3) or DMSO (inhibitor PI-4) and tested at various dilutions to determine the minimum concentration that effectively abolished needle assembly. Samples were mixed by pipet, incubated at room temperature for 5 min, then a 3 µl aliquot transferred to

a microscope slide and topped with a cover slip to minimize evaporation. Samples were visualized on an Olympus BX51 or Zeiss Axio Imager microscope equipped with Nomarski differential interference contrast optics. All micrographs were taken under similar illumination at $100\times$ or $200\times$ magnification.

Numbering of Residues

The numbering of residues in the crystal structures is derived from the protein sequence, which lacks the initiating methionine. Residue positions cited in the mutational study and the current work are based on the open reading frame of the gene sequence, including the initial methionine, and are $+1$ relative to those reported for the crystal structures.

REFERENCES

Baker AM, Roberts TM, Stewart M. 2002. 2.6 Å resolution crystal structure of helices of the motile major sperm protein (MSP) of *Caenorhabditis elegans*. J Mol Biol 319:491–499.

Berman HM, Westbrook J, Feng Z, Gilliland G, Bhat TN, Weissig H, Shindyalov IN, Bourne PE. 2000. The protein data bank. Nucleic Acids Res 28:235–242.

Bullock TL, Roberts TM, Stewart M. 1996. 2.5 Å resolution crystal structure of the motile major sperm protein (MSP) of *Ascaris suum*. J Mol Biol 263:284–296.

Burke DJ, Ward S. 1983. Identification of a large multigene family encoding the major sperm protein of *Caenorhabditis elegans*. J Mol Biol 171:1–29.

Buttery SM, Ekman GC, Seavy M, Stewart M, Roberts TM. 2003. Dissection of the *Ascaris* sperm motility machinery identifies key proteins involved in major sperm protein-based amoeboid locomotion. Mol Biol Cell 14:5082–5088.

Carlsson F, Brown EJ. 2006. Actin-based motility of intracellular bacteria, and polarized surface distribution of the bacterial effector molecules. J Cell Physiol 209:288–296.

Disanza A, Steffen A, Hertzog M, Frittoli E, Rottner K, Scita G. 2005. Actin polymerization machinery: The finish line of signaling networks, the starting point of cellular movement. Cell Mol Life Sci 62:955–970.

Haaf A, Butler PJ, Kent HM, Fearnley IM, Roberts TM, Neuhaus D, Stewart M. 1996. The motile major sperm protein (MSP) from *Ascaris suum* is a symmetric dimer in solution. J Mol Biol 260:251–260.

Haaf A, LeClaire L III, Roberts G, Kent HM, Roberts TM, Stewart M, Neuhaus D. 1998. Solution structure of the motile major sperm protein (MSP) of *Ascaris suum*— Evidence for two manganese binding sites and the possibile role of divalent cations in filament formation. J Mol Biol 284:1611–1624.

Italiano JE, Jr., Roberts TM, Stewart M, Fontana CA. 1996. Reconstitution *in vitro* of the motile apparatus from the amoeboid sperm of *Ascaris* shows that filament assembly and bundling move membranes. Cell 84:105–114.

King KL, Stewart M, Roberts TM, Seavy M. 1992. Structure and macromolecular assembly of two isoforms of the major sperm protein (MSP) from the amoeboid sperm of the nematode, *Ascaris suum*. J Cell Sci 101:847–857.

King KL, Stewart M, Roberts TM. 1994. Supramolecular assemblies of the *Ascaris suum* major sperm protein (MSP) associated with amoeboid cell motility. J Cell Sci 107:2941–2949.

Klass MR, Kinsley S, Lopez LC. 1984. Isolation and characterization of a sperm-specific gene family in the nematode *Caenorhabditis elegans*. Dev Biol 93:152–164.

LeClaire L III, Stewart M, Roberts TM. 2003. A 48 kDa integral membrane phosphoprotein orchestrates the cytoskeletal dynamics that generate amoeboid cell motility in *Ascaris* sperm. J Cell Sci 116:2655–2663.

Miao L, Yi K, Mackey JM, Roberts TM. 2007. Reconstitution in vitro of MSP-based filopodium extension in nematode sperm. Cell Motil Cytoskeleton 64:235–247.

Miller MA, Nguyen VS, Lee MH, Kosinski M, Schedl T, Caprioli RM, Greenstein D. 2001. A sperm cytoskeletal protein that signals oocyte meiotic maturation and ovulation. Science 291:2144–2147.

Morris MC, Robert-Hebmann V, Chaloin L, Mery J, Heitz F, Devaux C, Goody RS, Divita G. 1999. A new potent HIV-1 reverse transcriptase inhibitor: A synthetic peptide derived from the interface subunit domains. J Biol Chem 274:24941–24946.

Nelson GA, Roberts TM, Ward S. 1982. *Caenorhabditis elegans* spermatozoan locomotion: Amoeboid movement with almost no actin. J Cell Biol 92:121–131.

Pettersen EF, Goddard TD, Huang CC, Couch GS, Greenblatt DM, Meng EC, Ferrin TE. 2004. UCSF Chimera—A visualization system for exploratory research and analysis. J Comput Chem 25:1605–1612.

Pollard TD, Borisy GG. 2003. Cellular motility driven by assembly and disassembly of actin filaments. Cell 112:453–465.

Roberts TM, Ward S. 1982. Centripetal flow of pseudopodial surface components could propel the amoeboid movement of *Caenorhabditis elegans* spermatozoa. J Cell Biol 92:132–138.

Roberts TM, Pavalko FM, Ward S. 1986. Membrane and cytoplasmic proteins are transported in the same organelle complex during nematode spermatogenesis. J Cell Biol 102:1787–1796.

Roberts TM, Sepsenwol S, Ris H. 1989. Sperm notility in nematodes: Crawling movement without actin. In: Schatten H, Schatten G, editors. The cell biology of fertilization. New York: Academic Press, Inc. pp 41–60.

Rodriguez MA, LeClaire LL III, Roberts TM. 2005. Preparing to move: Assembly of the MSP amoeboid motility apparatus during spermiogenesis in *Ascaris*. Cell Motil Cytoskeleton 60:191–199.

Ruan B, Fisher KE, Alexander PA, Doroshko V, Bryan PN. 2004. Engineering subtilisin into a fluoride-triggered processing protease useful for one-step protein purification. Biochemistry 43:14539–14546.

Scott AL, Dinman J, Sussman DJ, Ward S. 1989. Major sperm protein and actin genes in free-living and parasitic nematodes. Parisitology 98:471–478.

Sepsenwol S, Ris H, Roberts TM. 1989. A unique cytoskeleton associated with crawling in the amoeboid sperm of the nematode, *Ascaris suum*. J Cell Biol 108:55–66.

Shakes DC, Ward S. 1989. Initiation of spermiogenesis in *C. elegans*: A pharmacological and genetic analysis. Dev Biol 134:189–200.

Smith HE, Ward S. 1998. Identification of protein–protein interactions of the major sperm protein (MSP) of *Caenorhabditis elegans*. J Mol Biol 279:605–619.

Stevens JM, Galyov EE, Stevens MP. 2005. Actin-dependent movement of bacterial pathogens. Nat Rev Microbiol 4:91–101.

Stewart M, King KL, Roberts TM. 1994. The motile major sperm protein (MSP) of *Ascaris suum* forms filaments constructed from two helical subfilaments. J Mol Biol 243:60–71.

Studier FW. 1991. Use of bacteriophage T7 lysozyme to improve an inducible T7 expression system. J Mol Biol 219:37–44.

Ward S, Klass M. 1982. The location of the major sperm protein in *Caenorhabditis elegans* sperm and spermatocytes. Dev Biol 92:203–208.

Ward S, Argon Y, Nelson GA. 1981. Sperm morphogenesis in wild-type and fertilization-defective mutants *of Caenorhabditis elegans*. J Cell Biol 91:26–44.

Ward S, Burke DJ, Sulston JE, Coulson AR, Albertson DG, Ammons D, Klass M, Hogan E. 1988. Genomic organization of major sperm protein genes and pseudogenes in the nematode *Caenorhabditis elegans*. J Mol Biol 199:1–13.